IEEE Access
Multidisciplinary | Rapid Review | Open Access Journal

Received 18 February 2023, accepted 4 March 2023, date of publication 6 March 2023, date of current version 15 March 2023.

Digital Object Identifier 10.1109/ACCESS.2023.3253680

RESEARCH ARTICLE

SNR Threshold-Based Relay Association and Random Phase Rotation for Cooperative Communication

JINGON JOUNG[1], (Senior Member, IEEE), SOOBUM PARK[2], JI-MYUNG OH[2], AND EUI-RIM JEONG[3], (Member, IEEE)

[1]School of Electrical and Electronics Engineering, Chung-Ang University, Seoul 06974, South Korea
[2]LIG Nex1, Giheung-gu, Yongin-si, Gyeonggi-do 16911, South Korea
[3]Department of Artificial Intelligence Software, Hanbat National University, Daejeon 34158, South Korea

Corresponding authors: Jingon Joung (jgjoung@cau.ac.kr) and Eui-Rim Jeong (erjeong@hanbat.ac.kr)

This work was supported in part by the Korea Research Institute for Defense Technology Planning and Advancement-Grant funded by the Defense Acquisition Program Administration (DAPA, 50%) under Grant KRIT-CT-21-030; in part by the Institute of Information and Communications Technology Planning and Evaluation (IITP) Grant funded by the Korea Government (MSIT) (Development of 5G Industrial Terminal Technology Supporting 28 GHz Band/Private 5G Band/NR-U Band, 20%) under Grant 2022-0-00635; and in part by the National Research Foundation of Korea (NRF) Grant funded by the Korea Government (MSIT) under Grant 2022R1A2C1003750 and Grant 2021R1A4A2001316.

ABSTRACT In this study, a cooperative communication system that employs multiple decode-and-forward relay nodes (RNs), in which the associated/active RNs perform phase rotation of the regenerated signals before retransmitting them to a destination node (DN), is examined. In the first phase, i.e., communication from a source node to RNs, a received signal-to-noise ratio (SNR) threshold-based RN association method is proposed. The optimal SNR thresholds are designed to maximize the bit-error-rate (BER) performance at the DN under various communication environments, such as modulation types and channel code rates. Furthermore, the number of phase rotations (PRs) in a frame is examined. Intensive numerical results show that more PRs in a frame provide better BER performance at the DN, irrespective of the communication environments. This study provides a valuable guideline for designing practical cooperative networks with multiple decode-and-forward RNs with PRs.

INDEX TERMS Cooperative communications, decode-and-forward relays, phase rotation, frame structure design.

I. INTRODUCTION

For the last few decades, to improve the performance of wireless communication between a source node (SN) and destination node (DN), cooperative communications that employ a relay node (RN) have been extensively studied [1], [2], [3], [4], [5], [6], [7], [8], [9], [10], [11], [12], [13], [14], [15], [16], [17], [18], [19], [20], [21], [22], [23], [24], [25], [26], [27], [28]. The applications of RN have recently extended from the traditional terrestrial nodes to the non-terrestrial nodes, such as the unmanned aerial vehicles [29] and satellites [30]. Various types of relaying protocols and relays exist.

According to the duplex methods, RNs can be classified as full-duplex and half-duplex. A full-duplex RN simultaneously retransmits and receives signals, whereas a half-duplex RN receives and transmits signals at different times. Because the full-duplex RN receives and transmits signals using the shared time and channel, it can provide higher spectral efficiency; however, the enormous gap between the retransmitted and received signals causes a critical issue, namely, severe self-interference in the full-duplex RN. To resolve this issue, many self-interference-mitigation methods have been studied [21], [25], [26], [31], [32]. By contrast, because there is no

The associate editor coordinating the review of this manuscript and approving it for publication was Prakasam Periasamy.

self-interference between retransmitted and received signals at the half-duplex RN, it can be readily implemented and has been actively studied [1], [13], [16], [18], [19], [20], [24], [22], [27], [28].

Moreover, according to the retransmission methods, amplify-and-forward (A&F) and decode-and-forward (D&F) are two representative types of relays. An A&F RN amplifies and forwards (retransmits) the received signals, whereas a D&F RN decodes and encodes the message from the received signals (i.e., regeneration) and forwards the regenerated signals [33]. Because the A&F RN merely retransmits the received signals from the SN to DN, the additive white Gaussian noise (AWGN) at the RN is also retransmitted to the DN. Therefore, many studies on A&F RN have focused on enhancing the intended signal strength in the second-hop channels [18], [21], [23], [24], [25], [26], [27]. However, second-hop channel state information (CSI) is required at the RN, which would burden the cooperative networks. By contrast, the D&F RN requires more computational capability and consumes relatively more power compared to the A&F RN, and the incorrectly decoded message signals interfere with the message recovery at the DN [13], [15], [16], [19], [22]. To reduce the decoding complexity at the D&F RN, a preprocessing-and-forward (PF)-type RN that detects the message symbols and processes them at the symbol level before the retransmission with less computational complexity has been proposed [20], [28]. Considering the massive distribution of battery-operated sensor RNs, the heavy computation for decoding and preprocessing may shrink the cooperative network size owing to the limited energy capability of the energy-hungry sensor RNs. Therefore, to extract the benefit of the RNs, two main issues should be carefully considered: i) the low-computational complexity of the D&F RN and ii) determining whether the D&F RN retransmits (decodes and forwards).

To resolve the main issues of a half-duplex D&F RN, a random phase rotation (PR), also known as phase dithering, scheme was proposed [34]. PR schemes can improve the diversity gain of multiple channels [15], [35], [36], [37], [38], [39]. In [36], the PR was applied to the multiple subcarriers of an orthogonal frequency-division multiple access system using an A&F relay. Here, the PR was amalgamated with the subcarrier permutation, and a novel signaling scheme that can eliminate the signaling overhead of the permutation was proposed. The PR was designed for the permutated subcarriers with no CSI, yet the subcarrier permutation requires the second-hop CSI at the relay node. On the other hand, instead of multiple subcarriers, multiple channels of multiple D&F RNs were used to extract the benefit of PR without any CSI of the second-hop channels. Concretely, the multiple RNs rotate the random phase of the regenerated signals before the retransmission [34], [35], [37], [38]. Consequently, the effective second-hop channel, which is the sum of the rotated second-hop channels, varies. Because multiple D&F RNs rotate the independent phase of their regenerated signals, the effective channel gain could achieve a spatial diversity gain at the DN. As no overhead for the second-hop CSI is required, the PR can be readily implemented at the D&F RNs. However, performing PR and retransmission is still challenging for RNs because the system does not know which RNs successfully decode and can join the retransmission [34], [35]. To resolve the abovementioned issue, an error-correcting code, i.e., cyclic redundancy check (CRC), was employed by the RNs. However, the CRC requires additional computation over the decoding computation. Moreover, the frequency with which the PRs need to be performed is unclear.

In this study, we answer two questions on the phase-rotated D&F RN strategy: i) which RNs perform retransmission? and ii) how many PRs are required? A low-computational-complexity signal-to-noise ratio (SNR) threshold-based RN activation policy is proposed to answer the first question. The proposed SNR threshold-based policy activates RNs whose received SNR in the first phase is greater than the threshold. By designing a proper SNR threshold, cooperation gain can be achieved. To answer the second question, the bit error rate (BER) is evaluated under various environments, and the observation of the number of PRs is provided; it is verified that the more the number of rotations provided, the better is the BER performance. This study would be a valuable guideline for designing cooperative networks with multiple half-duplex D&F RNs with PRs. The contributions of this study are summarized as follows:

- An SNR-based RN activation method is proposed and examined for cooperative communication systems with a PR scheme.
- A trade-off is shown to exist between interference and path loss while designing the SNR threshold to activate RNs.
- The guideline to design an SNR threshold for RN activation is provided.
- A trade-off is shown to exist between diversity gain and CSI estimation accuracy while designing the optimal number of PRs.
- A guideline to design the optimal number of PRs is provided.
- Intensive numerical results are provided to design two critical parameters in the cooperative communication systems:
  SNR threshold for RN activation should be carefully designed according to the modulation size, channel code rate, and number of PRs in a frame.
  PR number within a frame should be identical to the number of pilot symbols in the frame to improve BER performance.

The remainder of this paper is organized as follows. Section II describes the cooperative communication system model, including the frame structure and signal models. The proposed RN association method using an SNR threshold and the message detection and retransmission are presented in Section III. In Section IV, the design of two critical parameters, namely, the SNR threshold for RN activation and the

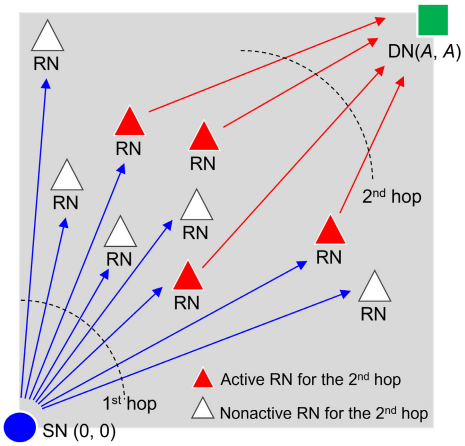

FIGURE 1. Cooperative network model with $\overline{K}$ half-duplex decode-and-forward (D&F) relay nodes (RNs) for communication between one source node (SN) and one destination node (DN). Here, K RNs are active for the retransmission. In this example, $\overline{K} = 9$ and $K = 4$.

number of PRs at RNs is described. Further, the BER performance of the proposed system is evaluated and compared with the benchmarking schemes under various communication environments in Section V. Finally, Section VI provides the conclusion.

Notations: The notation $|x|$ denotes the absolute value of x. $x \sim \mathcal{U}(a, b)$ means that a real-valued random variable x conforms to a uniform distribution between a and b; $x \sim \mathcal{CN}(0, \sigma^2)$ means that a complex random variable x conforms to a complex normal distribution with a zero mean and variance σ^2. E$[x]$ represents the mean of the random variable x.

II. SYSTEM AND SIGNAL MODELS

A. COOPERATIVE COMMUNICATION SYSTEM MODEL

In this study, the cooperative network illustrated in Fig. 1 was examined. One SN is located at $(0, 0)$ m, and a DN is located at (A, A) m in the Cartesian coordinate system. The SN transmits a single-stream message/information symbol to the DN through all or part of $\overline{K}$ RNs. Here, each node, namely, SN, RN, and DN, is assumed to have a single antenna. Moreover, the RNs are assumed to be half-duplex D&F relays and uniformly located at (x, y) m, where $x, y \sim \mathcal{U}(A, A)$. In the first phase, an SN transmits the sequence of the message symbols through the first-hop channels. Among $\overline{K}$ RNs, K RNs whose received SNR is greater than or equal to a certain predetermined threshold, η, decode and regenerate the message symbols, where $K \leq \overline{K}$. In the second phase, the K active RNs retransmit the regenerated message symbols to the DN through the second-hop channels. Hereinafter, the RNs involved in the retransmission in the second phase are referred to as *active RN*. The critical parameter definitions for the system model are summarized in Table 1.

B. FRAME STRUCTURE AND CHANNELS

The SN transmits T frames, each of which comprises $(S + 1)$ slots as illustrated in Fig. 2. The first slot, i.e., slot 0, includes

TABLE 1. Key parameter definitions of the considered system (alphabetic order).

Parameter	Definition
T	Number of frames
$\overline{K}$	Number of all relay nodes in networks
K	Number of active relay nodes
M	Modulation size of QAM
N	Number of message symbols per frame
Q	Number of pilot symbols per frame
R	Code rate of convolutional encoder
S	Number of message slots/phase rotations in a frame
η	Received SNR threshold (dB)
P_{SN}	Transmit power of SN
P_{RN}	Transmit power of RN
$g_{(k,t)}$ $(g_{(k)})$	Channel between SN and RN k (of frame t)
$h_{(k,t)}$ $(h_{(k)})$	Channel between RN k and DN (of frame t)
$\tilde{g}_{(k)}$	Estimate of $g_{(k)}$
$\tilde{h}_{(k)}$	Estimate of $h_{(k)}$
$x_{(s,n)}$	The nth message symbol in the sth slot
$\overline{x}(k, s, n)$	Regenerated signal of $x_{(s,n)}$ at RN k
$r_{(k,s,n)}$	Received signal of the nth symbol in slot s at RN k
$y_{(s,n)}$	Received signal of the nth symbol in slot s at DN
$\theta_{(k,s)}$	Phase rotation for slot s at RN k

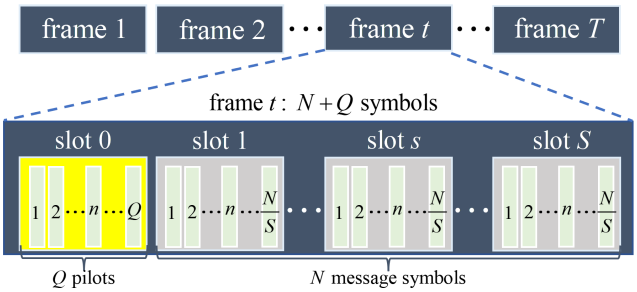

FIGURE 2. Illustration of the tth frame that comprises one pilot and S message slots.

Q pilot symbols, followed by S message slots, namely, slots 1–S. Each message slot includes $\frac{N}{S}$ symbols and is preprocessed before the transmission, i.e., PR. For notation simplicity, N is assumed to be a multiple of S. The slot-by-slot PR method will be introduced later.

The first-hop channel coefficient of frame t between the SN and RN k is modeled as a Rayleigh fading channel and denoted by $g_{(k,t)}$ as follows:

$$g_{(k,t)} = \sqrt{\xi_{S,k}}\bar{g}_{(k,t)}, \ k \in \overline{\mathcal{K}}, \ t \in \mathcal{T}, \tag{1}$$

where $\overline{\mathcal{K}} = \{1, \ldots, \overline{K}\}$ and $\mathcal{T} = \{1, \ldots, T\}$ are the sets of RN and block indices, respectively, $\xi_{S,k}$ is a large-scale fading between the SN and RN k, and $\bar{\boldsymbol{g}}_{(t,k)} \sim \mathcal{CN}(0, 1)$. Here, f_c is the carrier frequency. Similarly, the second-hop channel coefficient between the RN k and DN is also modeled as a Rayleigh fading channel and denoted by $h_{(k,t)}$ as follows:

$$h_{(k,t)} = \sqrt{\xi_{k,D}}\bar{h}_{(k,t)}, \ k \in \overline{\mathcal{K}}, \ t \in \mathcal{T}, \tag{2}$$

where $\xi_{k,D}$ is a large-scale fading between the RN k and DN, and $\bar{\boldsymbol{h}}_{(t,k)} \sim \mathcal{CN}(0, 1)$.

The channel coefficients $g_{(k,t)}$ and $h_{(k,t)}$ are static within a frame and vary independently of different frames, i.e., a block fading channel. Here, the frame size T is the same as the size of block channel coding.

C. SIGNAL MODELS

To avoid clutter, henceforth, the block index t is omitted as the signal processing for one block is independent of others.

The nth symbol of the sth slot is denoted by $x_{(s,n)}$, where, without loss of generality, $\mathrm{E}\left[|x_{(s,n)}|^2\right] = 1$, $s \in \mathcal{S} = \{0, \ldots, S\}$. Here, the 0th slot comprises the pilot symbols, denoted by $p_{(s,n)}$, and $n \in \{1, \ldots, Q\}$; Further, slot s, where $s \geq 1$, consists of $\frac{N}{S}$ message symbols, denoted by $d_{(s,n)}$, i.e.,

$$x_{(s,n)} = \begin{cases} p_{(0,n)}, & s = 0 \text{ and } n \in \{1, \ldots, Q\}, \\ d_{(s,n)}, & s \in \{1, \ldots, S\} \text{ and } n \in \left\{1, \ldots, \dfrac{N}{S}\right\}, \end{cases} \tag{3}$$

where, without loss of generality, it is assumed that $p_{(0,n)} = 1$, $\forall n \in \{1, \ldots, Q\}$. Thus, the transmitted signals from SN are as follows:

$$\Big[\underbrace{\underbrace{1 \cdots 1}_{Q \text{ pilots}}}_{\text{slot 0: pilots}} \quad \underbrace{\underbrace{x_{(1,1)} \cdots x_{\left(1,\frac{N}{S}\right)}}_{\text{slot 1: } \frac{N}{S} \text{ message symbols}} \cdots \underbrace{x_{(S,1)} \cdots x_{\left(S,\frac{N}{S}\right)}}_{\text{slot } S\text{: } \frac{N}{S} \text{ message symbols}}}_{N \text{message symbols}}\Big]. \tag{4}$$

By denoting the received signal of the nth symbol in slot s at RN k as $r_{(k,s,n)}$, the received pilot signals at RN k in the first phase are then written as follows:

$$r_{(k,s,n)} = \sqrt{P_{SN}} g_{(k)} x_{(s,n)} + z_{(k,s,n)}, \tag{5}$$

where P_{SN} is the transmit power of SN and $z_{(k,s,n)} \sim \mathcal{CN}(0, \sigma^2)$ is an AWGN at RN k.

In the second phase, the received signals of the nth symbol in slot s at DN are modeled as follows:

$$y_{(s,n)} = \sum_{k \in \mathcal{K}} \sqrt{P_{RN}} h_{(k)} \bar{x}_{(k,s,n)} + v_{(s,n)}, \tag{6}$$

where $\mathcal{K} \subseteq \overline{\mathcal{K}}$ is an index set of RNs that retransmit in the second phase, P_{RN} is the transmit power of RN, $\bar{x}_{(k,s,n)}$ is the regenerated message signal of $x_{(s,n)}$ at RN k, and $v_{(s,n)} \sim \mathcal{CN}(0, \sigma^2)$ is an AWGN at DN. The retransmitted signal $\bar{x}_{(k,s,n)}$ in (6) is constructed at RN k as follows:

$$\bar{x}_{(k,s,n)} = \begin{cases} p'_{(0,n)}, & s = 0 \text{ and } n \in \{1, \ldots, Q\}, \\ \bar{d}_{(k,s,n)}, & s \in \{1, \ldots, S\} \text{ and } n \in \left\{1, \ldots, \dfrac{N}{S}\right\}, \end{cases} \tag{7}$$

where $p'_{(0,n)}$ is the pilot sequence and $\bar{d}_{(k,s,n)}$ denotes the decoded information bits of $d_{(s,n)}$ at RN k. Here, $p'_{(0,n)}$ is different from that in the first phase in (3) and (4), whereas it is common for all RNs in the second phase, whose design will be described in Section III-B.

III. PROPOSED RN ASSOCIATION AND PHASE ROTATION

This section proposes an RN association method in the first phase, and introduces a random PR for the retransmission.

A. PHASE 1: RELAY NODE ASSOCIATION AND DATA DETECTION

In this subsection, an SNR threshold-based RN association method is proposed. If the message symbols are incorrectly regenerated at RN k, i.e., $\bar{x}_{(k,s,n)} \neq x_{(s,n)}$ (or equivalently, $\bar{d}_{k,s,n} \neq d_{s,n}$) in (6), the RNs should not retransmit the incorrect message to SN. Otherwise, the incorrect messages interfere with SN in decoding the original messages. To circumvent the incorrect message retransmission, an error-detecting code, e.g., CRC, can be employed by the RNs [35], which prevents the RNs from retransmitting the regenerated symbols if non-negligible errors are detected after the CRC. Accordingly, the fidelity of the second communication phase can be improved. However, the CRC may increase the computational complexity and energy consumption at the energy-hungry RNs and shrink the cooperation of the networks, as stated in Section I. Therefore, a low-computational-complexity strategy based on a received SNR threshold is proposed to resolve this issue.

The SNR threshold-based RN activation strategy is intuitive and straightforward because it does not require any additional information to determine whether the RN is performing retransmission (active RN) or silent (nonactive RN). Denoting the SNR threshold by η, the policy to determine an activation indicator $i_k \in \{0, 1\}$ of RN k is as follows:

$$\text{RN Act. Policy I: } i_k = \begin{cases} 0, & \text{if } SNR_{(k)} < \eta, \\ 1, & \text{o.w.} \end{cases}, \ \forall k \in \overline{\mathcal{K}}, \tag{8}$$

where $i_k = 0$ and $i_k = 1$ denote a silent and active RN k, respectively. Here, the received SNR at RN k, $SNR_{(k)}$, can be readily estimated using the pilot signals (3) in (5) as follows:

$$\begin{aligned} SNR_{(k)} &= \frac{1}{\sigma^2} \left| \frac{1}{Q} \sum_{n=1}^{n=Q} r_{(k,0,n)} \right|^2 \\ &= \frac{1}{\sigma^2} \left| \frac{1}{Q} \sum_{n=1}^{n=Q} \left(\sqrt{P_{SN}} g_{(k)} p_{(0,n)} + z_{(k,0,n)} \right) \right|^2 \\ &= \frac{P_{SN}}{\sigma^2} \left| g_{(k)} + \frac{1}{Q\sqrt{P_{SN}}} \sum_{n=1}^{n=Q} z_{(k,0,n)} \right|^2 \\ &\approx \frac{P_{SN} |\tilde{g}_{(k)}|^2}{\sigma^2}, \ \forall k \in \overline{\mathcal{K}}, \end{aligned} \tag{9}$$

where $\tilde{g}_{(k)} \triangleq g_{(k)} + \frac{1}{Q\sqrt{P_{SN}}} \sum_{n=1}^{n=Q} z_{(k,0,n)}$ is the estimate of $g_{(k)}$. Here, for notation simplicity, a set of active RN indices is defined as $\mathcal{K} = \{k'\} \subseteq \overline{\mathcal{K}}$, where $i_{k'} = 1$ and $i_{k'} \in \overline{\mathcal{K}}$.

Following the policy in (8), the active RNs are determined. Here, η should be carefully designed to balance the tradeoff between correct decoding at RNs (with large η) and the

diversity gain from RNs (with small η). However, optimally designing η is formidable for RNs because they do not know the second-hop channels, $h_{(k)}$; furthermore, the SN has no CSI and the DN only has the second-hop CSI. Moreover, the RNs are transparent, i.e., the SN and DN do not know how many RNs operate and are active in the networks. Therefore, the observations and guidelines to numerically determine the proper η will be provided in Section IV, which is one of the main contributions of this study.

A benchmarking policy is introduced for comparison with Policy I in (8). The benchmarking policy is a simple random activation policy with an activation parameter α as follows:

$$\text{RN Act. Policy II: } i_k = \Phi,\ \forall k \in \overline{\mathcal{K}}, \tag{10}$$

where Φ is a random variable that conforms to a Bernoulli distribution with the activation parameter α, i.e., $\Phi = 1$ with a probability of $\alpha/100$ and $\Phi = 0$ with a probability $1-\alpha/100$. Following Policy II, $\alpha\%$ of RNs are randomly activated in the cooperative networks. Though the RNs following Policy II do not need to compute the received SNR in (9), they are required to estimate the first-hop channel $\tilde{g}_{(k)}$ in (9) to decode the message and regenerate it.

After the RN activation/association, the active RNs decode and regenerate the messages in slots 1–S. Accordingly, RN k equalizes the received signals using the estimated 1st-hop channel $\tilde{g}_{(k)}$ in (9) as follows ($k \in \mathcal{K}$, $s = \{1, \ldots, S\}$, and $n = \{1, \ldots, N/S\}$):

$$\begin{aligned}\frac{1}{\sqrt{P_{SN}}\tilde{g}_{(k)}} r_{(k,s,n)} &= \frac{\sqrt{P_{SN}}g_{(k)}x_{(s,n)} + z_{(k,s,n)}}{\sqrt{P_{SN}}\tilde{g}_{(k)}} \\ &= \frac{g_{(k)}}{\tilde{g}_{(k)}}x_{(s,n)} + \frac{1}{\sqrt{P_{SN}}\tilde{g}_{(k)}} z_{(k,s,n)} \\ &\approx \tilde{x}_{(k,s,n)} \\ &\triangleq \bar{x}_{(k,s,n)},\end{aligned} \tag{11}$$

where $\tilde{x}_{(k,s,n)}$ is the estimated message symbol of $x_{(s,n)}$ at RN k and $\bar{x}_{(k,s,n)}$ is the regenerated message symbol, that is, one obtained by demodulating $\tilde{x}_{(k,s,n)}$ and modulating (regenerating) it again.

B. PHASE 1: RANDOM PHASE ROTATION AT RELAY NODES AND DATA DETECTION AT DESTINATION NODE

In the second phase, the active RNs retransmit the regenerated signals to the DN. To obtain spatial diversity gain by exploiting multiple channels between RNs and the DN, the PR scheme proposed in [35] is applied to each slot independently. The random phase that rotates the symbols in slot s of RN k is denoted by $\theta_{(k,s)}$, where $\theta_{(k,s)} \sim \mathcal{U}(-\pi, \pi)$, i.e., the random phases are between $-\pi$ and π and different for different RNs and slots, namely, k and s. Applying the random PR to the retransmitted signals, the retransmitted signal frame of RN k is structured as follows ($\forall k \in \mathcal{K}$):

$$\Big[\overbrace{\underbrace{e^{j2\pi\theta_{(k,1)}}\cdots e^{j2\pi\theta_{(k,1)}}}_{\text{group 1: } \frac{Q}{S} \text{ pilots for slot 1}} \cdots \underbrace{e^{j2\pi\theta_{(k,S)}}\cdots e^{j2\pi\theta_{(k,S)}}}_{\text{group } S\text{: } \frac{Q}{S} \text{ pilots for slot } S}}^{\text{slot 0: } Q \text{ pilot symbols}} \tag{12a}$$

$$\overbrace{e^{j2\pi\theta_{(k,1)}}\bar{x}_{(k,1,1)} \cdots e^{j2\pi\theta_{(k,S)}}\bar{x}_{\left(k,1,\frac{N}{S}\right)}}^{\text{slot 1: } \frac{N}{S} \text{ message symbols}} \tag{12b}$$

$$\vdots$$

$$\overbrace{e^{j2\pi\theta_{(k,S)}}\bar{x}_{(k,S,1)} \cdots e^{j2\pi\theta_{(k,s)}}\bar{x}_{\left(k,S,\frac{N}{S}\right)}}^{\text{slot } S\text{: } \frac{N}{S} \text{ message symbols}}\Big]. \tag{12c}$$

In the retransmitted frame of RN k shown in (12), the first part (12a) is a pilot sequence, i.e., slot 0. To estimate S effective channels that are rotated by S different phases, namely $\theta_{(k,1)}, \ldots, \theta_{(k,S)}$, the Q pilot symbols in (4) are grouped into S groups, each of which has $\frac{Q}{S}$ symbols. The pilot symbols in group τ are rotated by the same phase $\theta_{k,\tau}$ as in the message symbols as follows ($\tau = 1, \ldots, S$):

$$\begin{aligned}&\left[\bar{x}_{\left(k,0,(\tau-1)\frac{Q}{S}+1\right)}, \bar{x}_{\left(k,0,(\tau-1)\frac{P}{S}+2\right)}, \cdots, \bar{x}_{\left(k,0,\tau\frac{Q}{S}\right)}\right] \\ &\quad = \left[e^{j2\pi\theta_{(k,\tau)}},\ e^{j2\pi\theta_{(k,\tau)}},\ \cdots,\ e^{j2\pi\theta_{(k,\tau)}}\right] \in \mathbb{C}^{1\times\frac{Q}{S}}.\end{aligned} \tag{13}$$

The remaining parts of the frame shown in (12b) and (12c) are the regenerated message symbols at RN k, namely, $\bar{x}_{(k,1,1)}, \ldots, \bar{x}_{\left(k,1,\frac{N}{S}\right)}, \ldots,\ \bar{x}_{(k,S,1)}, \ldots, \bar{x}_{\left(k,S,\frac{N}{S}\right)}$ from slots 1 to S. Here, it can be assumed that the active RNs correctly decode the original messages throughout the RN association procedure described in the previous subsection. Under this assumption, the RN index k of the regenerated message symbols is dropped, that is, $\bar{x}_{(k,s,n)} = \bar{x}_{(s,n)},\ \forall k \in \mathcal{K}$.

After RN k's, where $k \in \mathcal{K}$, retransmit the frame in (12), the training parts of the received signals simultaneously at DN are written as

$$\begin{aligned}y_{\left(0,(\tau-1)\frac{Q}{S}+n\right)} &= \sum_{k\in\mathcal{K}} \sqrt{P_{RN}}h_{(k)}e^{j\theta_{(k,\tau)}} + v_{\left(0,(\tau-1)\frac{Q}{S}+n\right)} \\ &= f_{(\tau)} + v_{\left(0,(\tau-1)\frac{Q}{S}+n\right)}, \\ &\qquad \tau = 1, \ldots, S, \text{ and } n = 1, \ldots, \frac{P}{S},\end{aligned} \tag{14}$$

where $f_{(\tau)}$ is the effective channel that is involved in pilot group τ. Further, the message parts of the received signals at DN are written as

$$\begin{aligned}y_{(s,n)} &= \sum_{k\in\mathcal{K}} \sqrt{P_{RN}}h_{(k)}e^{j\theta_{(k,s)}}\bar{x}_{(s,n)} + v_{(s,n)} \\ &= f_{(s)}\bar{x}_{(s,n)} + v_{(s,n)}, \\ &\qquad 1 \le s \le S, \text{ and } 1 \le n \le \frac{N}{S},\end{aligned} \tag{15}$$

where $f_{(s)} = \sum_{k\in\mathcal{K}} \sqrt{P_{RN}}h_{(k)}e^{j\theta_{(k,s)}}$ is the effective second-hop channel of slot s.

Note that the effective channel gain for the coherence detection of $\bar{x}_{(s,n)}$ from (15) at the DN is different from that without the PR as given by

$$\|f_{(s)}\|^2 \neq \left\|\sum_{k\in\mathcal{K}} \sqrt{P_{RN}}h_{(k)}\right\|^2,\ \forall s \in \mathcal{S}, \tag{16}$$

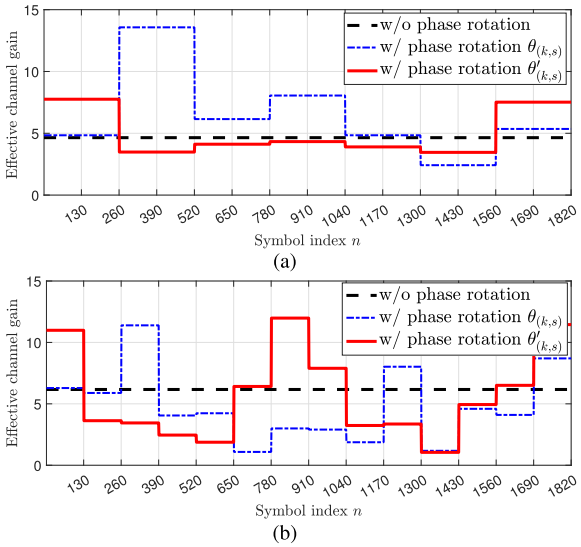

FIGURE 3. Illustration of the channel gains with and without phase rotation (PR) when $N = 1820$: (a) $S = 7$. (b) $S = 14$.

where the left- and right-hand sides are the effective channel gains with and without the PRs, respectively. To verify this result, the snapshots of the effective channel gains with and without the PRs are demonstrated in Fig. 3. As shown in Fig. 3, the effective channel gain without the PR is static within one frame comprising 1, 820 symbols, as assumed in the previous section. By contrast, the effective channel gains with the PRs vary over the slots ($S = 7$ and $S = 14$ slots in Figs. 3(a) and 3(b), respectively) as the PR is applied to each slot independently. To exploit the diversity gain from the varying channel gains, block channel coding and interleaving should be employed for the information bits within a frame.

The DN can readily estimate the second-hop effective channels for the slot s, i.e., the channels inside a norm of the left-hand side of (16), by averaging the received signals when $\tau = s$ in (14) as follows:

$$\begin{aligned}
&\frac{S}{Q}\sum_{n=1}^{n=\frac{Q}{S}} y_{\left(0,(s-1)\frac{Q}{S}+n\right)} \\
&= \frac{S}{Q}\sum_{n=1}^{n=\frac{Q}{S}}\left(\sum_{k\in\mathcal{K}}\sqrt{P_{RN}}h_{(k)}e^{j\theta_{(k,s)}} + v_{\left(0,(s-1)\frac{Q}{S}+n\right)}\right) \\
&= \sum_{k\in\mathcal{K}}\sqrt{P_{RN}}h_{(k)}e^{j\theta_{(k,s)}} + \frac{S}{Q}\sum_{n=1}^{n=\frac{Q}{S}} v_{\left(0,(s-1)\frac{Q}{S}+n\right)} \\
&\triangleq \tilde{f}_{(s)}. \qquad (17)
\end{aligned}$$

Using the estimate of the effective channel $\tilde{f}_{(s)}$ in (17), from the received signals in (15), the message symbols can be readily obtained as

$$\begin{aligned}
\frac{1}{\tilde{f}_{(s)}}y_{(s,n)} &= \frac{1}{\tilde{f}_{(s)}}\left(\sum_{k\in\mathcal{K}}\sqrt{P_{RN}}h_{(k)}e^{j\theta_{(k,s)}}\bar{x}_{(s,n)} + v_{(s,n)}\right) \\
&= \bar{x}_{(s,n)} + \frac{1}{\tilde{f}_{(s)}}v_{(s,n)} \\
&\triangleq \tilde{\bar{x}}_{(s,n)}. \qquad (18)
\end{aligned}$$

Remark 1: The computation for the relay selection is performed in each relay based on comparing the received SNR and a predetermined threshold η. Thus, the complexity for the relay selection (activation) of Policy I is merely measuring the received SNR in (9) and one comparison operation, which is relatively negligible compared to PR. Further, there is no additional computational complexity for the relay selection of Policy II in (10). On the other hand, the complexity of the PR at the active relays can be derived from (12). No operation is required for the pilot symbols in (12a), whereas N-complex-symbol multiplications are required for the PR of N message symbols. Thus, $\mathcal{O}(N)$ complexity is required once the relay is activated.

IV. DESIGN OF SNR THRESHOLD AND OPTIMAL NUMBER OF SLOTS/PHASE ROTATIONS

We designed the frame structure, including pilot slot 0 and message slots 1–S as shown in (12). The Q pilot symbols are grouped into S groups to estimate the S effective channels after the PR, with $\frac{Q}{S}$ pilots in each group of pilots. Because $\frac{Q}{S} \geq 1$, the number of PRs, i.e., slots, is restricted as $S \leq Q$ for a given length of pilot sequence Q. Under the fulfillment of $S \leq Q$, the diversity can be further exploited if the number of PRs increases. However, as S increases, the second-hop channel estimation accuracy decreases because the noise term increases, as shown in (17). Thus, the number of PRs (or equivalently, the number of slots) should be carefully designed.

The parameter configurations for the numerical example considered in this study are listed in Tables 2 and 3. Table 2 presents the possible numbers of slots, S, in addition, the corresponding pilot group length $\frac{Q}{S}$ and slot length $\frac{N}{S}$ are listed for $N = 1806$ and $Q = 14$. Table 3 lists the parameters for $N = 2304$ and $Q = 24$. The parameters in Tables 2 and 3 were used to determine the optimal number of PRs/slots in our simulation. The parameters are merely examples to provide the intuition to design a frame of the phase-rotated cooperative communication systems considered in this study.

To operate the proposed cooperative communication systems with the frames designed in Tables 2 and 3, we now design two essential system parameters, namely, an SNR threshold η to activate RNs and a slot number S to rotate the phase of the channels.

A. DESIGN OF SNR THRESHOLD, η, OF POLICY I TO ACTIVATE RELAY NODES

To design η, the number of active RNs was observed by varying η under various environments. The basic system parameters are summarized in Table 4. In a two-dimensional plane, the SN, RNs, and DN are located at (0, 0) m, (x, y) m, and (1200, 1200) m, respectively. In this study, the locations

TABLE 2. Frame design parameters when $N = 1806$ and $Q = 14$.

# of slots (S)	Pilot group length $\left(\frac{Q}{S}\right)$	Slot length $\left(\frac{N}{S}\right)$	Diversity gain	CSI accuracy
1	14	1806	↓	Increases
2	7	903	↓	↑
4	2	258	↓	↑
14	1	129	Increases	↑

TABLE 3. Frame design parameters when $N = 2304$ and $Q = 24$.

# of slots (S)	Pilot group length $\left(\frac{Q}{S}\right)$	Slot length $\left(\frac{N}{S}\right)$	Diversity gain	CSI accuracy
1	24	2304	↓	Increases
2	12	1152	↓	↑
3	8	768	↓	↑
4	6	576	↓	↑
6	4	384	↓	↑
8	3	288	↓	↑
12	2	192	↓	↑
24	1	96	Increases	↑

TABLE 4. Simulation environment.

Parameters	Values
SN position	$(0, 0)$ m
DN position	$A = 1200$, i.e., $(1200, 1200)$ m
RN position	(x, y) m, $x, y \sim \mathcal{U}(24, 1176)$
Distance btw. nodes A and B	$d_{A,B}$ m
Tx Pow. $P_{SN} = P_{RN}$	23 dBm or 32 dBm
Bandwidth	25 KHz
Noise figure	-174 dBm/Hz
Carrier frequency	2 GHz
Convolutional encoder	refer to Fig. 4
Code rate	$R = \frac{1}{2}$ and $R = \frac{2}{3}$
Interleaving	Random permutation
Fading	Rayleigh
Pathloss model	$-12.7-26\log_{10} f_c-36.7\log_{10} d_{A,B}$
Modulation	4-QAM, 16-QAM, 64-QAM
Total # of RNs	$5 \le \overline{K} \le 50$
# of RN realizations	1000
# of frames per RN realization	$T = 200$

of the RNs were uniformly distributed inside a 1152 $m \times$ 1152 m coverage area (refer to Fig. 6). The bandwidth was 25 KHz, and the carrier frequency was 2 GHz. The noise figure was assumed to be -174 dBm/Hz. Rate-$\frac{1}{2}$ 2^3-state and rate-$\frac{2}{3}$ 2^7-state non-recursive systematic convolutional encoders were employed [40]; their structure is shown in Fig. 4. After the channel coding, interleaving based on random permutation was conducted. Rayleigh fading channel was assumed, and the pathloss conformed to the 3GPP model in [41] and [42], i.e., $\xi_{A,B} = -12.7 - 26\log_{10}(f_c) - 36.7\log_{10}(d_{A,B})$, where $d_{A,B}$ is the distance between nodes A and B. A quadrature amplitude modulation (QAM) scheme was used for the modulation, namely, 4-QAM, 16-QAM, and 64-QAM. According to the

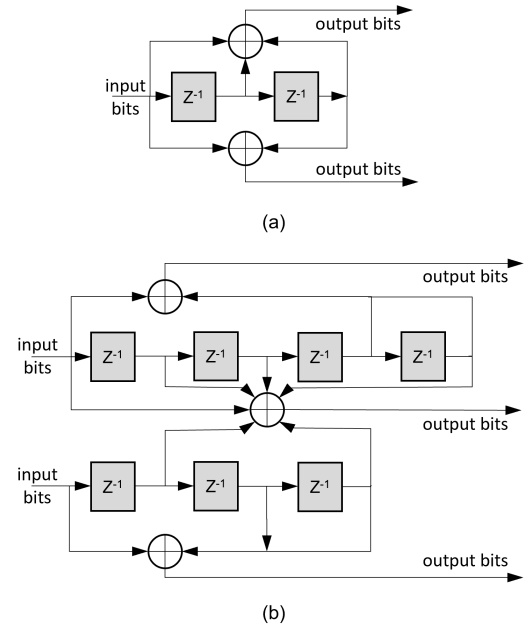

FIGURE 4. Nonrecursive systematic convolutional encoders: (a) Rate-1/2, 2^2 states. (b) Rate-2/3, 2^7 states.

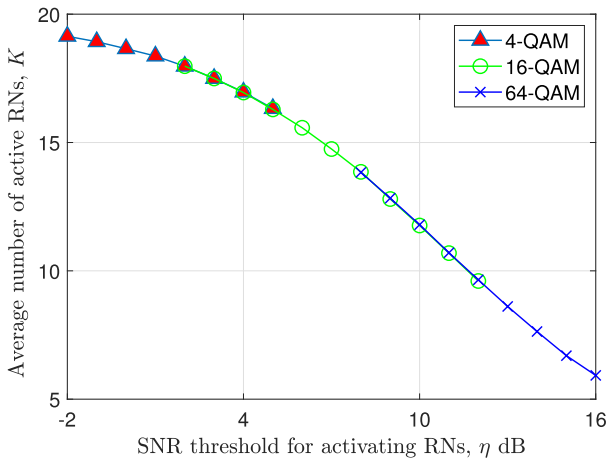

FIGURE 5. Number of active RNs K over η when there are total $\overline{K} = 20$ RNs (Policy I in (8)).

modulation scheme, the transmit power of SN and RNs was varied to obtain good BER performance of at least 10^{-1}. For a frame with $N = 1806$ in Table 2, $P_{SN} = P_{RN} = 23$ dBm is used for the 4-QAM and 16-QAM schemes, whereas $P_{SN} = P_{RN} = 32$ dBm is used for the 64-QAM scheme. For a frame with $N = 2304$ in Table 3, $P_{SN} = P_{RN} = 23$ dBm was used for the 4-QAM scheme, while $P_{SN} = P_{RN} = 32$ dBm was used for the 16-QAM and 64-QAM schemes. Here, it was assumed that $P_{SN} = P_{RN}$ as any of RNs could operate as an SN if multihop cooperation was considered. The total number of RNs was between 5 and 50. The structure of a frame of signals followed the parameters given in Tables 2 and 3. Two hundreds frames were transmitted once $\overline{K}$ RNs were realized.

Expectedly, as shown in Fig. 5, the number of active RNs decreases as the SNR threshold η increases when there are

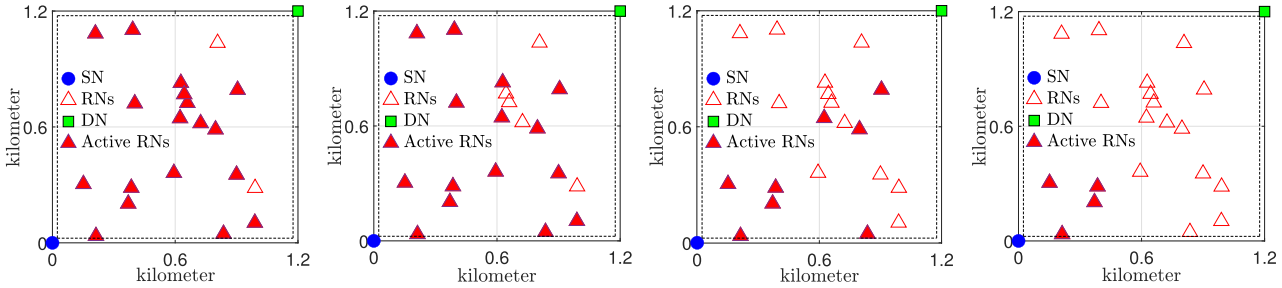

(a) $\eta = 2$ dB. (b) $\eta = 8$ dB. (c) $\eta = 14$ dB. (d) $\eta = 20$ dB.

FIGURE 6. Illustration of RN association from Policy I in (8) with various SNR thresholds η when $\overline{K} = 20$.

$\overline{K} = 20$ RNs. In particular, one SN, one DN, and $\overline{K} = 20$ RNs are generated, whose locations are marked by a blue circle, green square, and red triangles, respectively, in Fig. 6. The 20 RNs are located inside the area boxed by a dashed line following the distribution given in Table 4.

As shown in Fig. 6, the number of active RNs decreases from $K = 18$ to $K = 15$, $K = 8$, and $K = 4$ when η is increased from 2 to 8, 14, and 12 *dB*, respectively. Evidently, the number of active RNs, K, decreases as η increases because the number of RNs that fulfill the SNR threshold decreases, and it is independent of the modulation size M. Here, for the activation of RNs, the distance between SN and RN is not necessarily short, as clearly shown in Fig. 6(c), owing to the small-scale fading. The active RNs that are very far from the SN could be the *interference* sources because of the incorrect detection in the first phase, which observed in Fig. 6(a) with small η ($\eta = 2$ *dB*). However, the message signals of the activate RNs that are very far from the DN are successfully delivered to the DN with a low probability because of the large *path loss*, which is the case in Fig. 6(d) with a large η ($\eta = 20$ *dB*) because majority of the active RNs are very far from the DN. Consequently, as discussed in Section III-A, a trade-off exists between interference and path loss while designing η. Clearly, η is a critical design parameter for extracting the benefit of RNs in cooperative networks, and an optimal η exists for the communication environment.

To determine, η, the BER performance was evaluated for various environments, including modulation size M-QAM, channel code rate R, and the number of slots/PRs S. Each message symbol included $R \log_2 M$ bits of information. Here, S was set to the maximum value, i.e., $S = Q$. Later, it will be shown that a larger S provides better BER performance as the diversity gain improvement is major compared to the minor performance reduction caused by CSI accuracy reduction.

In Fig. 7(a), the BER performance is evaluated over η when the channel code rate $R = 1/2$, $N = 1806$, and $S = Q = 14$. As inferred in Section III-A, an optimal SNR threshold η to activate RNs exists. For example, the optimal SNR threshold η to determine the activation/retransmission of RNs is approximately 7 *dB* when $S = 14$, $R = 1/2$, and $M = 4$. Based on the results, the optimal SNR thresholds for specific slot number S, code rate R, and modulation size M are listed in Table 5.

In Fig. 7(c), the frame length N and slot number S are increased to $N = 2304$ and $S = Q = 24$, respectively. A comparison of the BERs of the PR systems in Figs. 7(a) and 7(c) reveals that the BER performance is improved as the number of slots, i.e., equivalently, the number of PRs in a frame, increases regardless of the modulation size, M. This observation is relevant within a fixed-length frame. In other words, the largest S would provide the best BER performance for a fixed-length frame.

In Figs. 7(b) and 7(d), code rate $R = 2/3$ is used in the simulation. Results similar to those in Figs. 7(a) and 7(c) with $R = 1/2$ can be observed. As the code rate was increased from $R = 1/2$ to $R = 2/3$, the message bits became more vulnerable to noise. Thus, the SN and RN transmit power was increased to 34 *dBm* for 16-QAM and 64-QAM to obtain a BER performance of at least 10^{-1}. The optimal SNR thresholds for activating RNs in the first phase are also listed in Table 5.

The guidelines obtained from this subsection are summarized in the remarks below:

Remark 2: A more extended frame size $N + Q$ provides better BER performance. To this end, the frame size can be determined such that the frame transmission time is the same as the coherence time of the channels.

Remark 3: More PRs (S) provide better BER performance; therefore, S is designed to have the maximum value that is the same as the number of pilot symbols, i.e., $S = Q$.

Remark 4: The SNR threshold η for activating RNs should be carefully designed according to the modulation size M, code rate R, and PR number S. Modulation size is a critical parameter for designing η. For examples, please refer to Table 5.

B. DESIGN OF THE NUMBER OF SLOTS, S, FOR PHASE ROTATIONS

In this subsection, the designing of the number of slots, i.e., the number of PRs, S, is described. As discussed at the beginning of this section, there exists a trade-off between the diversity gain and CSI accuracy when designing S. To obtain the optimal S, the BER performance is evaluated over S

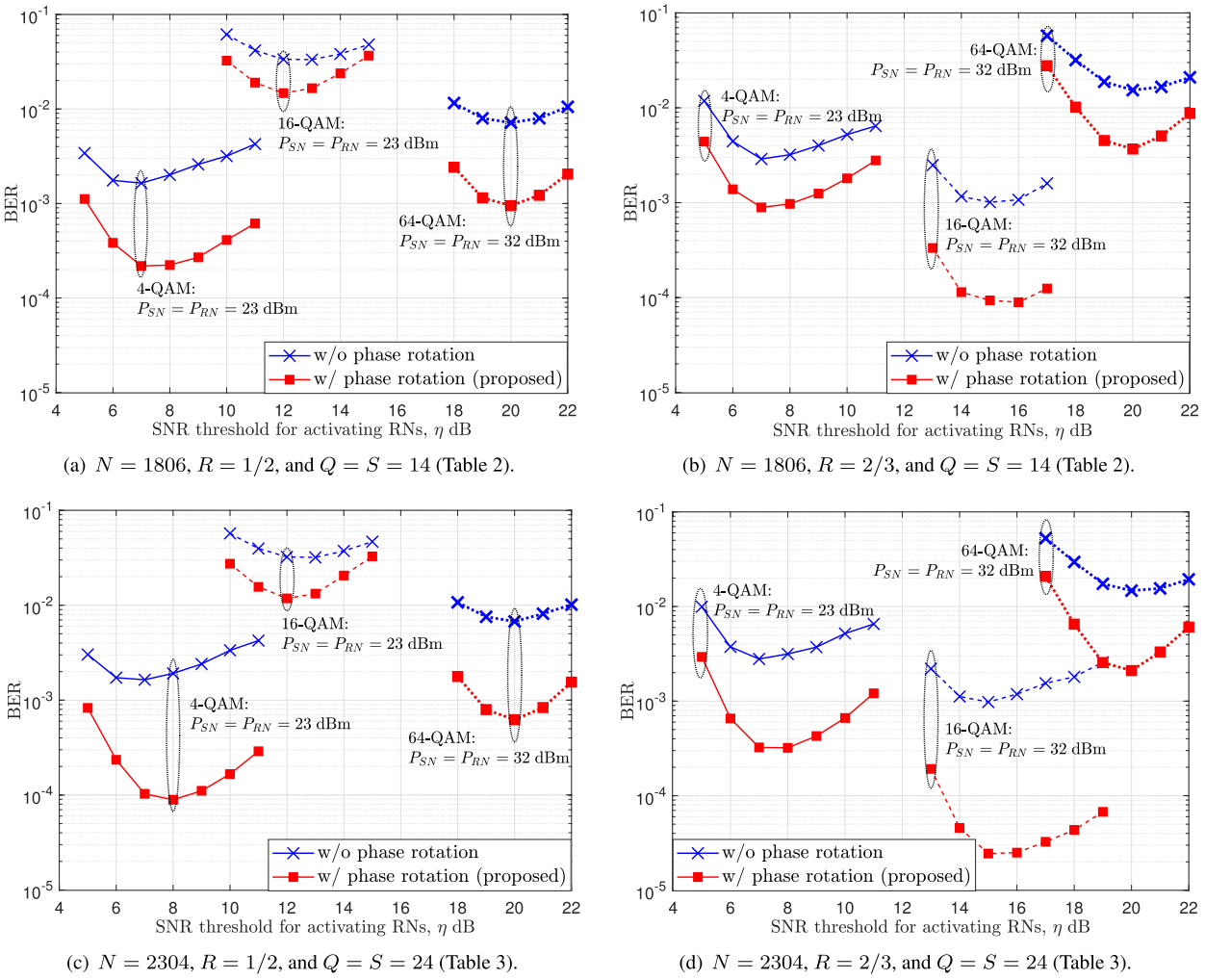

(a) $N = 1806$, $R = 1/2$, and $Q = S = 14$ (Table 2).

(b) $N = 1806$, $R = 2/3$, and $Q = S = 14$ (Table 2).

(c) $N = 2304$, $R = 1/2$, and $Q = S = 24$ (Table 3).

(d) $N = 2304$, $R = 2/3$, and $Q = S = 24$ (Table 3).

FIGURE 7. BER performance over the SNR threshold, η *dB*, under various environments: N, R, and S.

TABLE 5. System parameters for BER evaluation over η in Fig. 7 and for the transmit power $P_{SN} = P_{RN}$ *dBm* in Fig. 9.

System parameters					Optimal SNR	BER	BER	BER
# of message symbols	# of Pilots	Max. slot #	Code rate	Mod. size	Threshold	over η	over S	over P_{SN}=P_{RN}
$N = 1806$ (One frame length: $N + Q = 1830$)	$Q = 14$	$S = 14$	$R = 1/2$	$M = 4$	$\eta = 7$ dB	Fig. 7(a)	Fig. 8(a)	Fig. 9(a)
				$M = 16$	$\eta = 12$ dB			Fig. 9(b)
				$M = 64$	$\eta = 20$ dB			Fig. 9(c)
			$R = 2/3$	$M = 4$	$\eta = 7$ dB	Fig. 7(b)	Fig. 8(b)	Fig. 9(d)
				$M = 16$	$\eta = 16$ dB			Fig. 9(e)
				$M = 64$	$\eta = 20$ dB			Fig. 9(f)
$N = 2304$ (One frame length: $N + Q = 2328$)	$Q = 24$	$S = 24$	$R = 1/2$	$M = 4$	$\eta = 8$ dB	Fig. 7(c)	Fig. 8(c)	Fig. 9(g)
				$M = 16$	$\eta = 12$ dB			Fig. 9(h)
				$M = 64$	$\eta = 20$ dB			Fig. 9(i)
			$R = 2/3$	$M = 4$	$\eta = 8$ dB	Fig. 7(d)	Fig. 8(d)	Fig. 9(j)
				$M = 16$	$\eta = 15$ dB			Fig. 9(k)
				$M = 64$	$\eta = 20$ dB			Fig. 9(l)

with various parameters, including modulation size M, code rate R, and frame structure, as listed in Tables 2 and 3. For each environment, the best SNR threshold ηs obtained in the previous subsection, as given in Table 5, were used to determine the active RNs in the first phase. Other parameters were the same as those used in Fig. 7.

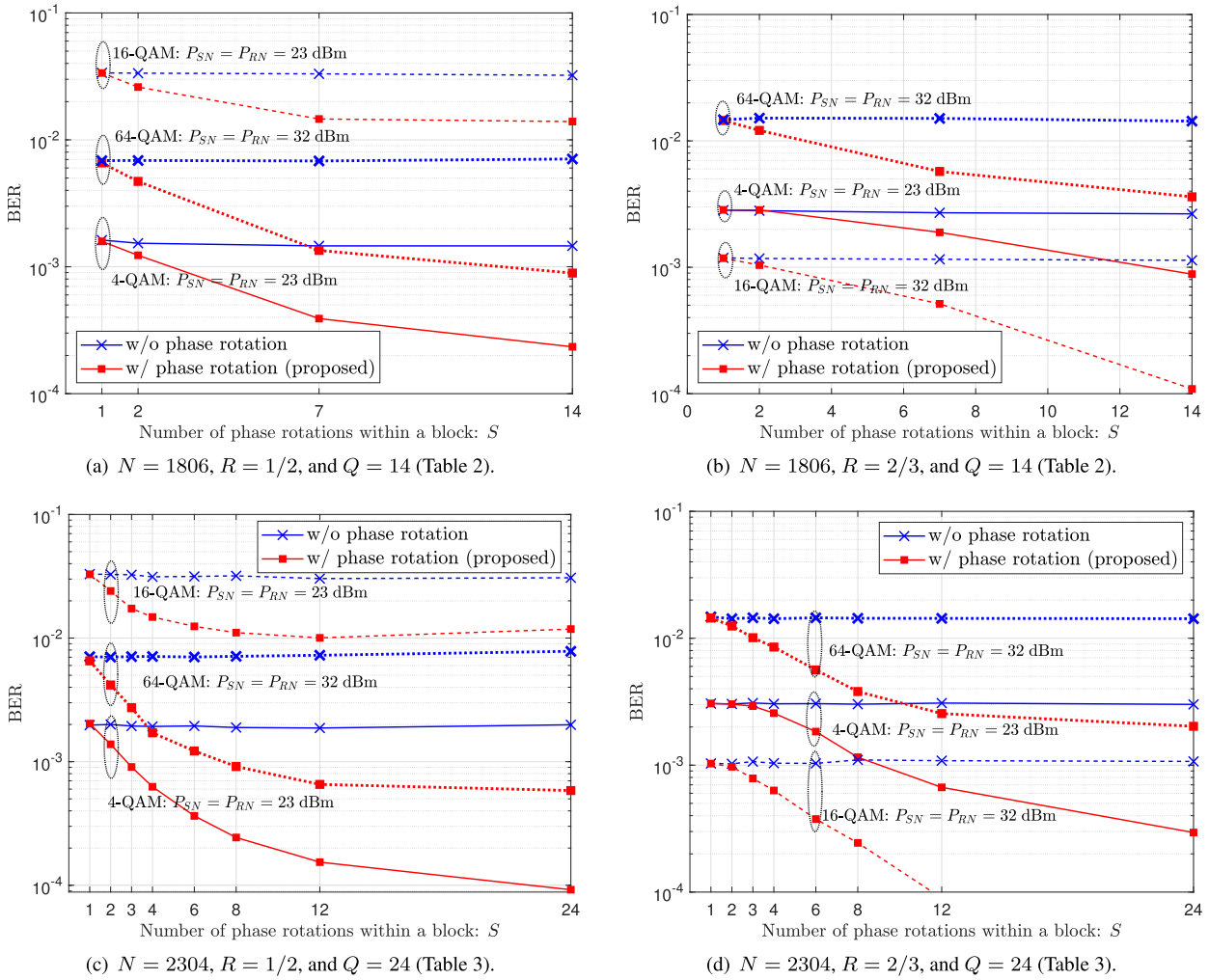

(a) $N = 1806$, $R = 1/2$, and $Q = 14$ (Table 2).

(b) $N = 1806$, $R = 2/3$, and $Q = 14$ (Table 2).

(c) $N = 2304$, $R = 1/2$, and $Q = 24$ (Table 3).

(d) $N = 2304$, $R = 2/3$, and $Q = 24$ (Table 3).

FIGURE 8. BER performance according to the number of PRs, S, under various environments: N, R, and Q.

A comparison of the BERs of 4-QAM in Fig. 8(a) with those in Fig. 8(b) reveals that a higher code rate decreases the BER performance. Similar results are observed for 64-QAM between Figs. 8(a) and 8(b) and between Figs. 8(c) and 8(d). For 4-QAM and 64-QAM, $P_{SN} = P_{RN} = 23$ dB and $P_{SN} = P_{RN} = 32$ dB, respectively, were used. Note that $P_{SN} = P_{RN} = 23$ dB was used for 16-QAM schemes shown in Figs. 8(a) and 8(c), while $P_{SN} = P_{RN} = 32$ dB was used for those shown in Figs. 8(b) and 8(d) for obtaining reliable BER results under 10^{-1}.

The results shown in Fig. 8 indicate that the BER of the RNs without the PR is almost stable. However, the BER performance is generally improved as the number of PRs, S, increases. These results are aligned with the observation in Section IV-A. As stated in Remark 3, a larger number of slots, i.e., the number of PRs, is better for BER performance. Thus, the number of PRs, S, should be equal to the maximum available number, i.e., the number of PRs should be equal to the length of the pilot sequence, $S = Q$.

V. BER PERFORMANCE COMPARISON

The BER performance of the proposed phase-rotated cooperative communication systems employing the designed η and S was compared with benchmarking systems. The compared systems are as follows:

- **All RNs without PR** (benchmarking scheme): All RNs in the network retransmit signals without PR.
- **All RNs with PR** (benchmarking scheme): All RNs in the network retransmit signals after PR.
- **Random RNs without PR** (benchmarking scheme): α of RNs are randomly selected (Policy II in (10)) and retransmit signals without PR. Here, $\alpha = 30\%$, which is found such that the best BER is obtained in general.
- **Random RNs with PR** (benchmarking scheme): $\alpha = 30\%$ of RNs are randomly selected and retransmit signals after PR.
- **Active RNs without PR** (benchmarking scheme): Designed SNR threshold-based RN association is employed, yet PR is not employed.

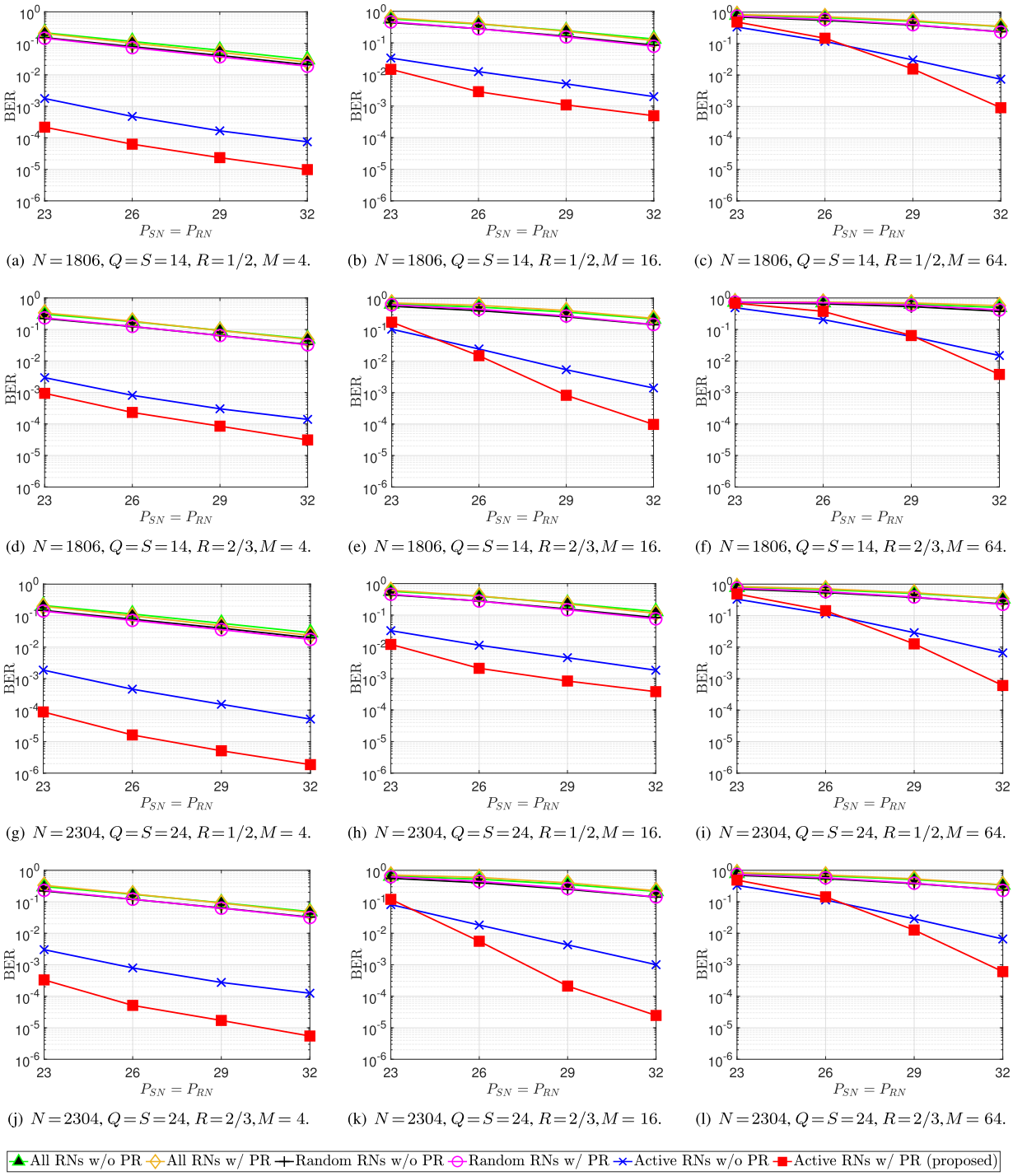

(a) $N=1806, Q=S=14, R=1/2, M=4$. (b) $N=1806, Q=S=14, R=1/2, M=16$. (c) $N=1806, Q=S=14, R=1/2, M=64$.

(d) $N=1806, Q=S=14, R=2/3, M=4$. (e) $N=1806, Q=S=14, R=2/3, M=16$. (f) $N=1806, Q=S=14, R=2/3, M=64$.

(g) $N=2304, Q=S=24, R=1/2, M=4$. (h) $N=2304, Q=S=24, R=1/2, M=16$. (i) $N=2304, Q=S=24, R=1/2, M=64$.

(j) $N=2304, Q=S=24, R=2/3, M=4$. (k) $N=2304, Q=S=24, R=2/3, M=16$. (l) $N=2304, Q=S=24, R=2/3, M=64$.

FIGURE 9. BER performance according to transmit power $P_{SN} = P_{RN}$ under various environments: N, R, M, and $Q = S$.

- **Active RNs with PR** (proposed scheme): Designed SNR threshold-based RN association and PR employed by active RNs.

A. BER PERFORMANCE ACCORDING TO TRANSMIT POWER

Figure 9 shows BER performance evaluation according to transmit power $P_{SN} = P_{RN}$ under various system environments listed in Table 5. The transmit power considered in the simulation was between 23 to 32 *dBm*. Two types of frame structures, given in Tables 2 and 3, were considered. For the channel coding, the convolutional encoders shown in Fig. 4 were employed with $R = 1/2$ and $R = 2/3$. Further, the best received SNR threshold ηs in Table 5 and the maximum number of PRs, i.e., $S = Q$, were considered for the proposed active RNs with or without PR. Three types

of QAM, namely, 4-QAM, 16-QAM, and 64-QAM, were employed.

As expected, the BER performance was generally improved as the transmit power increased for all compared schemes. The benchmarking schemes, namely All RNs and Random RNs, exhibited poor BER performance because the correct message recovery in the first-hop communication was not guaranteed. Thus, the PR did not effectively improve the BER performance as well. By contrast, the proposed Active RN schemes achieved good BER performance as they carefully considered the first-hop channel quality, i.e., the received SNRs at RNs, by comparing it with η. Consequently, the PR could effectively improve the BER performance at the DN, particularly when the modulation size and code rate were small, i.e., 4-QAM in Fig. 9(a). As the code rate increased from $R = 1/2$ (Fig. 9(a)) to $R = 2/3$ (Fig. 9(b)), the failure probability of the message recovery increased in the first phase, resulting in the reduction of the PR effect in the second phase. As the modulation size increased (from the figures in the left to the right column), the BER performance generally decreased. The BER performance of the proposed Active RNs with PR was worse than that of Active RNs without PR if the modulation size was high, code rate was high, or the transmit power was insufficient, i.e., if the first-hop communication quality was insufficient for the cooperation (e.g., $\{M = 64,\ R = 1/2,\ P_{SN} = P_{RN} = 23\ dBm\}$ in Fig. 9(c), $\{M = 16,\ R = 2/3,\ P_{SN} = P_{RN} = 23\ dBm\}$ in Fig. 9(e), and $\{M = 64,\ R = 2/3,\ P_{SN} = P_{RN} = 23\ dBm\}$ in Fig. 9(f)). However, the proposed Active RNs with PR generally outperformed all benchmarking schemes.

Figures 9(g)–(l) show BER performance evaluation for a long frame with $N = 2304$. The long-frame BER trend is similar to that for a short frame with $N = 1806$ in Figs. 9(a)–(f). Comparison of the BERs in Figs. 9(a)–(f) with those in Figs. 9(g)–(l) verifies Remark 2 (Section IV-A), i.e., the more extended frame size provides better BER performance. Furthermore, the BER performance improvement obtained from PR increases with the longer frame (compare the BER gap between Active RNs with and without PR in Fig. 9(d) with that in Fig. 9(j)) because the longer frame rotates phase much more frequently (i.e., the longer frame has a larger S.).

From the results in Fig. 9, the following remark is presented as a guidelines to design the proposed Active RNs with PR:

Remark 5: To effectively achieve diversity gain from multiple active RNs, a small modulation size or sufficient transmit power is required.

B. BER PERFORMANCE ACCORDING TO THE TOTAL NUMBER OF RELAY NODES

In this section, we verify that the proposed method can improve BER performance regardless of the total number of RNs, $\overline{K}$. Two environments are considered: one is a low-data-rate mode with $M = 4$ and $R = 1/2$ (Fig. 10(a)) and the other one is a high-data-rate mode with $M = 64$ and $R = 2/3$ (Fig. 10(b)). A short frame is considered in both cases: $N = 1806$ and $Q = 14$.

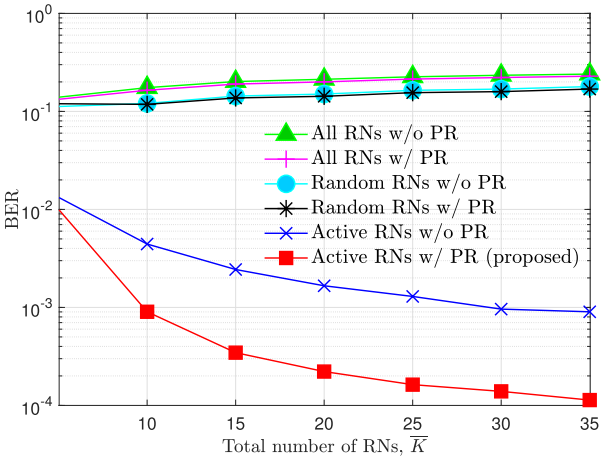

(a) Low-data-rate mode.

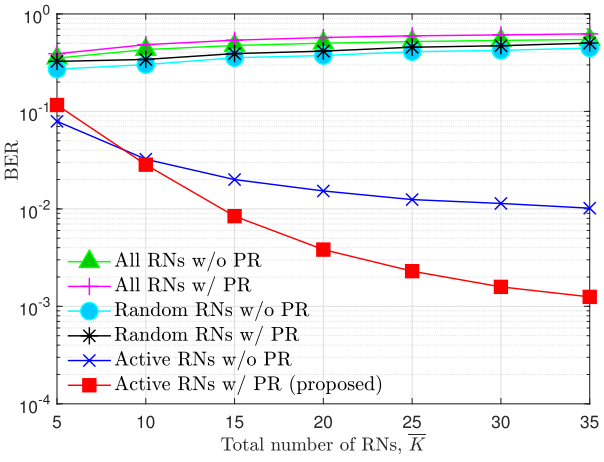

(b) High-data-rate mode.

FIGURE 10. BER performance according to the total number of RNs, $\overline{K}$, when $N = 1806$ and $Q = S = 14$: (a) A low-data-rate mode: $M = 4$ and $R = 1/2$. (b) A high-data-rate mode: $M = 64$ and $R = 2/3$.

A comparison of the results in Figs. 10(a) and 10(b) indicates that BER performance decreases as the transmission rate increases. Furthermore, as expected, the BER of Active RN methods decreases as $\overline{K}$ increases. However, interestingly, the BER performances of the All and Random RN schemes deteriorate as $\overline{K}$ increases. RNs could harm the cooperation unless they are carefully operated, as they can be an interference source rather than a cooperation source. From the results, it is also verified that the BER performance can be improved throughout the PR at RNs, regardless of the number of RNs, if the active RNs are properly associated with the cooperation.

VI. CONCLUSION

In this study, a frame structure including a pilot slot is designed for a cooperative communication system, and a received SNR threshold-based RN association method and a phase rotation scheme are examined. From the intensive

numerical results, a valuable guideline to design the practical cooperative networks with multiple decode-and-forward RNs with phase rotations is provided as four remarks: i) The more extended frame size provides the better BER performance; ii) The more frequent phase rotations provides the better BER performance; iii) The SNR threshold for activating RNs should be carefully designed according to the modulation size, code rate, and phase rotation number; and iv) To effectively achieve the diversity gain from multiple active RNs, either a small modulation size or sufficient transmit power is required. Though this study covers the example systems with the specific communication parameters and the guideline with remarks is numerically obtained from them, it would be helpful for future work to design the practical multiple D&F RNs with phase rotation in cooperative networks.

REFERENCES

[1] B. Rankov and A. Wittneben, "Spectral efficient protocols for half-duplex fading relay channels," *IEEE J. Sel. Areas Commun.*, vol. 25, no. 2, pp. 379–389, Feb. 2007.

[2] I. Hammerstrom, M. Kuhn, C. Esli, J. Zhao, A. Wittneben, and G. Bauch, "MIMO two-way relaying with transmit CSI at the relay," in *Proc. IEEE 8th Workshop Signal Process. Adv. Wireless Commun.*, Helsinki, Finland, Jun. 2007, pp. 1–5.

[3] K. G. Seddik and K. J. R. Liu, "Distributed space-frequency coding over broadband relay channels," *IEEE Trans. Wireless Commun.*, vol. 7, no. 11, pp. 4748–4759, Nov. 2008.

[4] V. Havary-Nassab, S. Shahbazpanahi, A. Grami, and Z.-Q. Luo, "Distributed beamforming for relay networks based on second-order statistics of the channel state information," *IEEE Trans. Signal Process.*, vol. 56, no. 9, pp. 4306–4316, Sep. 2008.

[5] M. M. Abdallah and H. C. Papadopoulos, "Beamforming algorithms for information relaying in wireless sensor networks," *IEEE Trans. Signal Process.*, vol. 56, no. 10, pp. 4772–4784, Oct. 2008.

[6] E. Koyuncu, Y. Jing, and H. Jafarkhani, "Distributed beamforming in wireless relay networks with quantized feedback," *IEEE J. Sel. Areas Commun.*, vol. 26, no. 8, pp. 1429–1439, Oct. 2008.

[7] W. Guan and H. Luo, "Joint MMSE transceiver design in non-regenerative MIMO relay systems," *IEEE Commun. Lett.*, vol. 12, no. 7, pp. 517–519, Jul. 2008.

[8] B. Khoshnevis, W. Yu, and R. Adve, "Grassmannian beamforming for MIMO amplify-and-forward relaying," *IEEE J. Sel. Areas Commun.*, vol. 26, no. 8, pp. 1397–1407, Oct. 2008.

[9] H. J. Yang and J. Chun, "Generalized Schur decomposition-based two-way relaying for wireless MIMO systems," in *Proc. IEEE Global Telecommun. Conf. (GLOBECOM)*, New Orleans, LA, USA, 2008, pp. 1–6.

[10] J. Joung and A. H. Sayed, "Power allocation for beamforming relay networks under channel uncertainties," in *Proc. IEEE Global Telecommun. Conf. (GLOBECOM)*, Honolulu, HI, USA, Nov. 2009, pp. 1–6.

[11] R. Zhang, Y.-C. Liang, C. C. Chai, and S. Cui, "Optimal beamforming for two-way multi-antenna relay channel with analogue network coding," *IEEE J. Sel. Areas Commun.*, vol. 27, no. 5, pp. 699–712, Jun. 2009.

[12] J. Joung and A. H. Sayed, "Multiuser two-way relaying method for beamforming systems," in *Proc. IEEE 10th Workshop Signal Process. Adv. Wireless Commun.*, Perugia, Italy, Jun. 2009, pp. 280–284.

[13] J. Joung and A. H. Sayed, "Multiuser two-way amplify-and-forward relay processing and power control methods for beamforming systems," *IEEE Trans. Signal Process.*, vol. 58, no. 3, pp. 1833–1846, Mar. 2010.

[14] V. Havary-Nassab, S. Shahbazpanahi, and A. Grami, "Optimal distributed beamforming for two-way relay networks," *IEEE Trans. Signal Process.*, vol. 58, no. 3, pp. 1238–1250, Mar. 2010.

[15] J. Joung and S. Sun, "Phase rotation and link selection methods for DSTTD-based two-path relay systems," *IEEE Commun. Lett.*, vol. 15, no. 3, pp. 278–280, Mar. 2011.

[16] J. Joung and S. Sun, "Power efficient resource allocation for downlink OFDMA relay cellular networks," *IEEE Trans. Signal Process.*, vol. 60, no. 5, pp. 2447–2459, May 2012.

[17] V. T. Muralidharan and B. S. Rajan, "Distributed space time coding for wireless two-way relaying," *IEEE Trans. Signal Process.*, vol. 61, no. 4, pp. 980–991, Feb. 2013.

[18] J. Joung and J. Choi, "Linear precoder design for an AF two-way MIMO relay node with no source node precoding," *IEEE Trans. Veh. Technol.*, vol. 66, no. 11, pp. 10526–10531, Nov. 2017.

[19] S. B. Roy, A. S. Madhukumar, and J. Joung, "On joint Pareto frontier in multiple access and relay rate regions with Rayleigh fading," *IEEE Trans. Veh. Technol.*, vol. 66, no. 5, pp. 3777–3786, May 2017.

[20] J. Joung, "Energy efficient space–time line coded regenerative two-way relay under per-antenna power constraints," *IEEE Access*, vol. 6, pp. 47026–47035, 2018.

[21] Y. Shao, L. Wang, and X. Cao, "On the performance of space–time block coded spatial modulation transmission for full-duplex relay networks," *IEEE Access*, vol. 7, pp. 180976–180985, 2019.

[22] J. Wei, J. Wei, S. Hu, and W. Chen, "Successive decode-and-forward relaying with privacy-aware interference suppression," *IEEE Access*, vol. 8, pp. 95793–95806, 2020.

[23] L. Han, R. Zhou, Y. Li, B. Zhang, and X. Zhang, "Power control for two-way AF relay assisted D2D communications underlaying cellular networks," *IEEE Access*, vol. 8, pp. 151968–151975, 2020.

[24] J. Joung and A. H. Sayed, "User selection methods for multiuser two-way relay communications using space division multiple access," *IEEE Trans. Wireless Commun.*, vol. 9, no. 7, pp. 2130–2136, Jul. 2010.

[25] S. A. A. Kazmi and S. Coleri, "Optimization of full-duplex relaying system with non-linear energy harvester," *IEEE Access*, vol. 8, pp. 201566–201576, 2020.

[26] H.-P. Dang, M.-S. Van Nguyen, D.-T. Do, H.-L. Pham, B. Selim, and G. Kaddoum, "Joint relay selection, full-duplex and device-to-device transmission in wireless powered noma networks," *IEEE Access*, vol. 8, pp. 82442–82460, 2020.

[27] J. Wang, Y.-C. Liang, J. Joung, X. Yuan, and X. Wang, "Joint beamforming and reconfigurable intelligent surface design for two-way relay networks," *IEEE Trans. Commun.*, vol. 69, no. 8, pp. 5620–5633, Aug. 2021.

[28] J. Choi and J. Joung, "Process-and-forward two-way relay using layered STBCs and multiple STLCs," *Signal Process.*, vol. 196, Jul. 2022, Art. no. 108526.

[29] J. Li, Y. Niu, H. Wu, B. Ai, R. He, N. Wang, and S. Chen, "Joint optimization of relay selection and transmission scheduling for UAV-aided mm wave vehicular networks," *IEEE Trans. Veh. Technol.*, early access, doi: 10.1109/TVT.2022.3233550.

[30] J. Li, G. Wu, T. Liao, M. Fan, X. Mao, and W. Pedrycz, "Task scheduling under a novel framework for data relay satellite network via deep reinforcement learning," *IEEE Trans. Veh. Technol.*, early access, doi: 10.1109/TVT.2022.3233358.

[31] B. Chun, E.-R. Jeong, J. Joung, Y. Oh, and Y. H. Lee, "Pre-nulling for self-interference suppression in full-duplex relays," in *Proc. Asia–Pacific Signal Inf. Process. Assoc., Annu. Summit Conf. (APSIPA)*, Sapporo, Japan, Oct. 2009, pp. 949–952.

[32] B. C. Nguyen, T. M. Hoang, L. T. Dung, and T. Kim, "Impacts of nonlinear energy harvesting and residual self-interference on the performance of full-duplex decode-and-forward relay system," *IEEE Access*, vol. 9, pp. 42333–42344, 2021.

[33] C. S. Patel and G. L. Stuber, "Channel estimation for amplify and forward relay based cooperation diversity systems," *IEEE Trans. Wireless Commun.*, vol. 6, no. 6, pp. 2348–2356, Jun. 2007.

[34] I. Harmerstriom, M. Kuhn, and A. Wittrieben, "Cooperative diversity by relay phase rotations in block fading environments," in *Proc. IEEE 5th Workshop Signal Process. Adv. Wireless Commun.*, Lisbon, Portugal, Jul. 2004, pp. 293–297.

[35] D. K. Lee and K. M. Chugg, "A pragmatic approach to cooperative communication," in *Proc. IEEE Mil. Commun. Conf. (MILCOM)*, Washington, DC, USA, Oct. 2006, pp. 1–7.

[36] M. Wen, X. Chen, Q. Li, E. Basar, Y.-C. Wu, and W. Zhang, "Index modulation aided subcarrier mapping for dual-hop OFDM relaying," *IEEE Trans. Commun.*, vol. 67, no. 9, pp. 6012–6024, Sep. 2019.

[37] Q.-U.-A. Nadeem, A. Zappone, and A. Chaaban, "Intelligent reflecting surface enabled random rotations scheme for the MISO broadcast channel," *IEEE Trans. Wireless Commun.*, vol. 20, no. 8, pp. 5226–5242, Aug. 2021.

[38] C. Psomas and I. Krikidis, "Low-complexity random rotation-based schemes for intelligent reflecting surfaces," *IEEE Trans. Wireless Commun.*, vol. 20, no. 8, pp. 5212–5225, Aug. 2021.

[39] K.-H. Lee, J. S. Yeom, J. Joung, and B. C. Jung, "Performance analysis of uplink NOMA with constellation–rotated STLC for IoT networks," *IEEE Open J. Commun. Soc.*, vol. 3, pp. 705–717, 2022.
[40] J. G. Proakis and M. Salehi, *Digital Communications*, 5th ed. New York, NY, USA: McGraw-Hill, 2007.
[41] J. Kim, J. Joung, and K. Lim, "Intelligent reflecting surface-aided space–time line coded systems," *IEEE Wireless Commun. Lett.*, vol. 11, no. 2, pp. 245–249, Feb. 2022.
[42] *Further Advancements for E-UTRA Physical Layer Aspects (Release 9)*, The 3rd Generation Partnership Project (3GPP TM), document TS 36.814, Mar. 2010.

JINGON JOUNG (Senior Member, IEEE) received the B.S. degree in radio communication engineering from Yonsei University, Seoul, South Korea, in 2001, and the M.S. and Ph.D. degrees in electrical engineering and computer science from the Korea Advanced Institute of Science and Technology (KAIST), Daejeon, South Korea, in 2003 and 2007, respectively.

He was a Postdoctoral Fellow with KAIST and the University of California at Los Angeles, Los Angeles, CA, USA, in 2007 and 2008, respectively. From 2009 to 2015, he was a Scientist with the Institute for Infocomm Research (I^2R), Agency for Science, Technology and Research (A*STAR), Singapore. He joined Chung-Ang University (CAU), Seoul, in 2016, as a Faculty Member. He is currently a Professor with the School of Electrical and Electronics Engineering, CAU, where he is also the Principal Investigator of the Intelligent Wireless Systems Laboratory. He is an Inventor of *Space–Time Line Code* that is a fully symmetric scheme for a space–time block code (Alamouti code). His research interests include wireless communication signal processing, numerical analysis, algorithms, and machine learning.

Dr. Joung was a recipient of the First Prize from the Intel-ITRC Student Paper Contest, in 2006, the TVT Top Editor Award, in 2021, and the IEIE Research Pioneer Award, in 2022. He was recognized as an Exemplary Reviewer of IEEE COMMUNICATIONS LETTERS, in 2012, and IEEE WIRELESS COMMUNICATIONS LETTERS, in 2012, 2013, 2014, and 2019. He was the Guest Editor of IEEE ACCESS, in 2016, an Editorial Board Member of the *APSIPA Transactions on Signal and Information Processing*, from 2014 to 2019, and an Editor of *Sensors*, in 2020. In addition, he has been an Associate Editor of IEEE TRANSACTIONS ON VEHICULAR TECHNOLOGY, from 2018 to 2023.

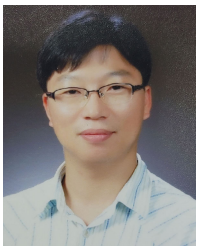

SOOBUM PARK received the B.S. degree in electrical engineering from the Korea Advanced Institute of Science and Technology (KAIST), Daejeon, South Korea, in 2001, and the M.S. degree from the School of Information and Communication, Hanyang University, Seoul, South Korea, in 2006. He is currently a Chief Research Engineer with the C4I Research and Development Center, LIG Nex1. His research interests include military communications, mobile ad hoc networks, and future wireless communication systems.

JI-MYUNG OH received the B.S. and M.S. degrees in radio science and engineering from Korea University, Seoul, South Korea, in 1997 and 1999, respectively. He is currently a Chief Research Engineer with the Department of Data-Link and Modem, LIG Nex1. His research interests include wireless communication systems and modem design.

EUI-RIM JEONG (Member, IEEE) received the B.S., M.S., and Ph.D. degrees from the Department of Electrical Engineering, Korea Advanced Institute of Science and Technology (KAIST), Daejeon, South Korea, in 1995, 1997, and 2001, respectively. He has been a Professor with the Department of Artificial Intelligence Software, Hanbat National University, since 2009. His research interests include communication signal processing, pre-distortion, and modem design.